Journal of Industrial and Management Optimization

https://www.aimspress.com/journal/jimo

JIMO, 22(10): 5351–5381.
DOI:10.3934/jimo.2026184
Received: 04 July 2026
Revised: 01 September 2026
Accepted: 18 September 2026
Published: 23 September 2026

Research article

A prescriptive analytics framework for service and carbon tradeoffs in disrupted supply chains

Ashish Chandra*

College of Business, Illinois State University, Normal, 61761, Illinois, USA

* **Correspondence:** Email: achand6@ilstu.edu; Tel: +1-309-438-3022.

Abstract: Supply chain networks (SCNs) are increasingly required to balance high service performance with low carbon emissions, while also remaining resilient to disruptions. Although both sustainability and disruption management have been widely studied, limited attention has been given to how disruptions affect the tradeoff between service and environmental performance. This paper examines how link failures reshape the service-carbon tradeoff in multi-echelon SCNs. We model the network as a capacitated flow system, where disruptions eliminate the capacity of failed links, and the service performance is measured by the total lost demand (TLD). Transportation-related carbon emissions are modeled as flow-dependent quantities, and a lexicographic ϵ-constraint approach is used to generate efficient service–carbon frontiers between the TLD and the total transportation-related carbon emissions (TCE). To capture severe operational conditions, the principal analysis selects a fixed adverse disruption scenario that maximizes the minimum TLD across all failure scenarios involving a given number of link failures, while additional experiments examine alternative fixed-scenario selection rules. Computational experiments on synthetically generated networks reveal changes in the marginal service recovery along the service–carbon tradeoff under disruption. Under the principal max–min adverse-scenario analysis, larger failure budgets are associated with worse service outcomes and generally earlier declines toward lower marginal-improvement levels. Additional experiments using critical-link, random, and representative-average random fixed disruption scenarios show that the magnitude of service degradation depends on the failed-link configuration, while the underlying service–carbon tradeoff and changing marginal effectiveness of additional emissions persist across the alternative scenario-selection rules. From a managerial perspective, these findings highlight the importance of both the network structure and the link criticality when planning sustainability-constrained recovery.

Keywords: supply chain disruptions; carbon emissions modeling; service level analysis; disruption modeling; multi-echelon networks; pareto optimization
Mathematics Subject Classification: 90B06, 90B20, 90C29

1. Introduction

Supply chain networks (SCNs) are increasingly required to achieve high levels of service performance while simultaneously reducing their environmental impact. Growing regulatory pressures, corporate sustainability commitments, and stakeholder expectations have made carbon efficient operations a central priority in supply chain management. At the same time, recent global events—including pandemics, geopolitical disruptions, and infrastructure failures—have highlighted the vulnerability of supply chains and the challenges of maintaining service continuity under adverse conditions. These dual pressures create a fundamental operational tension. Achieving higher service levels may require additional transportation activity and the use of alternative routing options, potentially increasing transportation-related carbon emissions. Conversely, restricting emissions limits the routing flexibility and can degrade the service performance. This tradeoff becomes even more pronounced under disruptions, where the network capacity is reduced and feasible routing options are constrained.

Although both sustainability and disruption management have received significant attention in the literature, these two dimensions are often studied separately. Sustainability focused research primarily examines emission reduction strategies under nominal operating conditions, while disruption focused studies analyze system performance degradation and recovery without explicitly accounting for environmental impact. As a result, there is limited understanding of how disruptions affect the tradeoff between service performance and transportation-related carbon emissions. In particular, an important and largely unexplored question is how disruption severity reshapes the service improvements attainable as the carbon emission limit is relaxed. When capacity is reduced due to disruptions, relaxing the carbon emission limit may allow greater use of available routing alternatives and thereby help restore service levels. However, it is unclear whether such additional transportation activity remains effective as the disruptions intensify, or whether structural constraints within the network limit its impact.

This paper addresses this gap by studying the service carbon tradeoff in multi-echelon SCNs under link failures. We model the supply chain as a capacitated network, where disruptions are represented as failures of transportation links that eliminate the available capacity. Service performance is measured using the total lost demand (TLD), which directly captures unmet customer demand, while transportation-related carbon emissions are measured using the transportation-related carbon emissions (TCE) generated by the network flows. For a given disruption scenario, we formulate an optimization problem that minimizes the TLD subject to an upper limit on the TCE. By systematically varying this emission limit using an ϵ-constraint approach, we generate service–carbon frontiers that characterize the best achievable tradeoffs between the service performance and the environmental impact. For the principal analysis, we select a fixed adverse disruption that maximizes the minimum TLD across all failure scenarios involving a prescribed number of failed links. Additionally, we examine alternative fixed scenario selection rules to assess the sensitivity of the service–carbon findings to the choice of disruption benchmark.

Our analysis distinguishes between structural properties implied by the optimization model and disruption dependent characteristics of the service–carbon frontier. Relaxing the emission limit necessarily expands the feasible routing set and therefore cannot worsen the optimal service performance; similarly, nested link removals cannot improve the optimal service level. Consequently, the central question of this study is not whether relaxing the emission limit can worsen service, but how much service improvement is obtained as the limit is relaxed and how the *marginal effectiveness* of additional permitted emissions changes under disruption. Our computational analysis examines changes in the marginal service improvement along the tradeoff and how these patterns vary with the disruption severity, network density, and network topology.

The contributions of this paper are threefold: first, we develop a network based lexicographic ϵ-constraint framework that integrates disruption induced capacity loss, service degradation, and flow-dependent transportation-related carbon emissions while ensuring that the reported service–carbon points are efficient; second, we characterize structural properties of the service–carbon value function and explicitly separate relationships implied by feasible set inclusion from the nontrivial shape characteristics of the frontier; and third, we use a marginal improvement analysis to quantify the service improvement per the additional unit of the TCE between consecutive efficient frontier points and examine how the disruption severity and the network structure affect the resulting marginal improvement profiles. This shifts the emphasis from the expected direction of the service–carbon relationship to the rate, persistence, and structural sensitivity of recovery along the frontier.

The remainder of the paper is organized as follows: Section 2 reviews the related literature; Section 3 presents the SCN model and problem formulation, and also describes the tradeoff framework and the proposed solution approach; Section 4 presents the experimental design and computational setup; Section 5 reports the results and managerial insights; and finally, Section 6 concludes the paper and outlines directions for future research.

2. Literature Review

This section positions the paper within the literature on sustainable supply chains, SCN disruption management, and multi objective optimization. While each of these streams has developed extensively, their intersection at the operational level remains comparatively limited. This motivates the present study, which examines how disruptions alter the tradeoff between service performance and carbon emissions. To identify literature most closely related to this study, we conducted a targeted review of peer reviewed research on four intersecting themes: (i) carbon aware and sustainable supply chain optimization, (ii) supply chain disruption and resilience, (iii) integrated sustainable resilient supply chain models, and (iv) network interdiction and multi-objective tradeoff analysis. Therefore, Table 1 provides a focused comparison of representative studies rather than an exhaustive bibliometric review.

Table 1. Focused comparison of representative literature related to the present study.

Study (Year)	Primary focus	Disruption sustainability scope	Distinction from the present study
[1] (2013)	Carbon aware supply chain operations	Carbon policies; no explicit disruptions	Examines carbon effects on operational decisions but not disruption induced service degradation.
[2] (2012)	Sustainable SCN design	Emission trading and environmental network design	Strategic design focus; does not analyze operational service–carbon frontiers under link failures.
[3] (2022)	Bi-objective green SCN design	Green network design under disruption risk	Integrates environmental & disruption considerations primarily at the network design level rather than analyzing post disruption service–carbon recovery.
[4] (2022)	Green resilient network design under uncertainty	Resilience, environmental performance, and route risk	Focuses on robust strategic network design rather than the operational TLD–TCE frontier of a fixed disrupted network.
[5] (2023)	Two-stage stochastic supply chain optimization	Facility/transport disruptions and operational uncertainty	Models disruption & recovery decisions but does not characterize the marginal service–carbon tradeoff.
[6] (2024)	Uncertain sustainable network design	Greenhouse gas emissions and uncertain network decisions	Emphasizes cost and sustainable network design rather than service degradation under adversarial link failures.
[7] (2025)	Scoping and bibliometric review	Sustainable and resilient SCN design	Synthesizes the design literature; does not develop an operational service–carbon frontier under disruptions.
[8] (2026)	Risk averse multi objective green network design	Cost emission tradeoffs under uncertainty	Addresses uncertainty aware green design rather than disruption induced capacity loss and TLD–TCE recovery.
[9] (2026)	Complex network and machine learning analysis	Cascading failures and critical state mitigation	Identifies and mitigates critical disruption states but does not analyze carbon constrained service recovery.
This study (2026)	Lexicographic ϵ-constraint & network interdiction	Link disruptions, TLD, and transportation related emissions	Examines how fixed adverse link disruptions reshape the operational service–carbon frontier and its marginal improvement profile.

Carbon aware supply chain optimization: A significant body of research incorporates carbon emissions into supply chain decision making. Early studies demonstrated that operational decisions such as production, transportation, and inventory control can substantially influence the carbon footprint of supply chains. For instance, prior research showed that carbon considerations can alter the optimal operational policies in managing supply chains [1], while other research integrated environmental objectives into inventory models [10]. At the network level, prior research examined the supply chain design under emission trading schemes and highlighted the impact of environmental regulations on the facility location and flow decisions [2]. Recently, an analytics framework for carbon aware supply chain routing was provided in [11]. In a related direction, inventory decisions under carbon constraints were studied by jointly optimizing cost and emissions [12]. However, this stream primarily examines carbon aware operations without explicitly modeling disruption induced service degradation. These studies establish the importance of carbon aware operations, but they are primarily developed under nominal conditions. The service performance is typically embedded within feasibility constraints or indirectly captured through cost based objectives. As a result, they do not explicitly analyze how the service levels deteriorate when environmental constraints interact with capacity disruptions.

Supply chain disruptions and resilience: Another stream of research focused on supply chain disruptions, reliability, and resilience. Early work emphasized strategies to mitigate supply chain disruptions [13], while subsequent studies examined network robustness and performance loss under facility or transportation failures [14–16]. Recent reviews synthesized the rapidly expanding literature on supply chain disruption and resilience [17–19]. Additionally, more recent work examined cascading failures and critical states in SCNs [9,20]. This literature provides important insights into how disruptions reduce feasible flows and degrade the service performance. However, in the disruption focused studies considered in this stream, the environmental performance is generally not the primary modeling dimension. Even when service metrics such as unmet demand or disruption costs are modeled, the carbon implications of recovery strategies are not incorporated. Consequently, these studies provide important insight into performance degradation and recovery under disruption but generally do not characterize the operational service–carbon frontier examined here.

Network interdiction and adverse disruption selection: Network interdiction provides a closely related optimization perspective to identify disruptions that most severely impair the network performance. In a typical interdiction model, an outer decision selects the network components to disable the subject to an interdiction constraint, while an inner problem represents the optimal response of the affected network. A comprehensive survey of network interdiction models and mathematical programming solution approaches was provided in [21], including formulations based on dualization [22, 23]. This structure is directly relevant to a supply chain disruption analysis when link failures are selected adversarially and the disrupted network subsequently reroutes flow optimally. The role of interdiction in the present study is narrower than designing a general purpose interdiction policy. It is used to construct a fixed adverse disruption benchmark by selecting f failed links that maximize the minimum achievable TLD under optimal recovery. Then, the selected failed network is held fixed while the service–carbon frontier is evaluated. Thus, the interdiction component determines the disrupted operating environment, whereas the primary analysis concerns how the service–carbon tradeoff evolves within that environment.

Integrated sustainable and resilient supply chain models: A growing body of work seeks to integrate sustainability and resilience within unified optimization frameworks. A recent scoping and bibliometric review documented the growing intersection between sustainable and resilient SCN design [7]. At the modeling level, prior research developed a bi-objective green SCN design model under disruption risk [3], while other research integrated environmental and resilience considerations in a green resilient network design under uncertainty [4]. Robust sustainable closed loop supply chains under alternative carbon emission schemes were examined in prior research [24], and a stochastic four-echelon supply chain model incorporating both disruptions and operational uncertainty was also developed [5]. More recent studies continue to extend uncertainty aware sustainable network optimization. Greenhouse gas emissions were considered in uncertain sustainable SCN design [6], while a risk averse multi-objective framework for green supply chain design under uncertainty was developed in related research [8]. Collectively, these studies demonstrate substantial progress toward integrating environmental and resilience considerations. However, their primary emphasis remains on strategic network design, uncertainty management, cost emission objectives, and the selection of resilience strategies. Instead, the present study fixes the network design and examines how disruption induced capacity loss changes the operational frontier between unmet demand and transportation related emissions. These models represent an important step toward unified sustainable and resilient supply chain analyses, but their emphasis is predominantly on strategic design, uncertainty management, cost emission, and resilience objectives rather than on characterizing the operational service–carbon frontier following capacity disruption. Moreover, disruptions are often modeled through scenario based or probabilistic approaches rather than through adversarial selection of operationally damaging link failure configurations.

Multi-objective optimization and tradeoff analysis: Multi-objective optimization methods are widely used to analyze tradeoffs across many engineering disciplines (for instance, see [25, 26]). In the supply chain context, the use of multi-objective optimization in sustainable SCN design has been reviewed in the literature [27]. More generally, constraint based approaches for generating Pareto solutions, including ϵ-constraint variants, have been developed and applied across different optimization settings [28, 29]. These approaches provide valuable tools to understand tradeoffs and support decision making. Related decision theoretic work, such as the tri-level framework of [30], further highlights the value of distinguishing among different decision regions when evaluating complex tradeoffs. However, most applications focus on either design stage decisions or nominal operations. The resulting tradeoffs typically involve cost, emissions, or responsiveness, rather than explicit measures of service degradation under disruptions. As a result, how disruption induced capacity loss affects operational service–carbon frontiers remains insufficiently explored.

Research gap and contribution: The literature reviewed above reveals three closely related gaps. First, carbon aware supply chain models generally do not characterize how disruption induced capacity loss changes the attainable relationship between service and transportation related emissions. Second, disruption and resilience models analyze performance loss and recovery but typically do not examine how environmental restrictions affect the attainable service response. Third, studies that integrated sustainability and resilience predominantly focused on strategic network design, uncertainty management, or cost–emission objectives rather than the operational shape of the service–carbon frontier after capacity loss. Network interdiction provides a natural mechanism to identify adverse network disruptions, but its role in the present study is complementary: interdiction is used to construct the disrupted operating environment whose subsequent service–carbon tradeoff is analyzed.

This paper addresses these gaps by studying the operational service–carbon tradeoff in a fixed multi-echelon SCN under link failures. Therefore, the analysis connects adverse disruption selection, service degradation, environmental performance, and marginal recovery behavior within a unified operational framework.

3. Methodology

This section presents the SCN model, the disruption framework, and the tradeoff formulation used to analyze the relationship between service performance and transportation-related carbon emissions.

Supply chain network structure: We consider a four-echelon SCN consisting of suppliers (S), plants (P), warehouses (W), and retailers (R). The network is represented as a directed graph $G(V, E)$, where $V = S \cup P \cup W \cup R$ and $E = E_{SP} \cup E_{PW} \cup E_{WR}$ denotes the set of links connecting consecutive echelons. This configuration is widely recognized in the SCN literature as a *four-echelon SCN* (for instance, see [5,31–34]). A fundamental assumption in our SCN configuration is that *demand exclusively occurs at the retail level*, with no fixed operational costs considered at any facility. These assumptions are consistent with standard formulations in multi-echelon supply chain configurations as stated in [14, 35]. Each link $\langle i, j\rangle \in E$ has a finite capacity $c_{ij} \geq 0$, and demand only occurs at the retail level. We let D_r denote the demand at retailer $r \in R$. Flow variables y_{ij} represent the quantity transported along each link, and unmet demand at retailer r is denoted by d_r. See Table 2 for the notational summary.

Table 2. Notational summary for the SCN models.

Symbol	Description
S, P, W, R	Known sets of supplier, plant, warehouse, and retailer nodes
V	Set of all nodes in the SCN, $V = S \cup P \cup W \cup R$
$s \in S, p \in P$	Indices for supplier s ($s \in S$) and plant p ($p \in P$)
$w \in W, r \in R$	Indices for warehouse w ($w \in W$) and retailer r ($r \in R$)
E_{SP}, E_{PW}, E_{WR}	Known set of edges: ($S \to P$), ($P \to W$), and ($W \to R$)
E	Set of all edges in the SCN, $E = E_{SP} \cup E_{PW} \cup E_{WR}$
$c_{ij} \in \mathbb{R}$	Known maximum capacity of edge $\langle i, j \rangle \in E$
$D_r \in \mathbb{R}$	Known demand requirement at retailer $r \in R$
m_{ij}	Transportation mode assigned to link $\langle i, j \rangle \in E$
ρ^m	Freight emission factor for transportation mode m
$\ell_{ij} \in \mathbb{R}_+$	Transportation distance of link $\langle i, j \rangle$ (miles)
$\eta_{ij} \in \mathbb{R}_+$	Link specific emission coefficient, $\eta_{ij} = \rho^{m_{ij}} \ell_{ij}$
ϵ	Upper limit on TCE
$\epsilon_{\text{Max}}(x)$	Minimum TCE required to attain the minimum achievable TLD under x
Decision Variable	Description
$y_{ij} \in \mathbb{R}_+$	Flow routed through edge $\langle i, j \rangle \in E$
$d_r \in \mathbb{R}_+$	Unmet demand at retailer node $r \in R$
$x_{ij} \in \{0, 1\}$	Failure indicator for link $\langle i, j \rangle$ (1 if failed, 0 otherwise) under failure scenario x
$\alpha_{ij} \in \mathbb{R}_+$	Dual variable associated with the capacity constraint for link $\langle i, j \rangle \in E$
$\gamma_p \in \mathbb{R}$	Free dual variable associated with flow conservation at plant $p \in P$
$\theta_w \in \mathbb{R}$	Free dual variable associated with flow conservation at warehouse $w \in W$
$\lambda_r \in \mathbb{R}$	Free dual variable associated with retailer demand balance at $r \in R$

Units: d, D, y, c (short tons); ℓ (miles); ρ (kg CO_2 per short-ton-mile); and TCE (kg CO_2).

Disruption modeling: Disruptions are modeled as link failures. Given a SCN failure scenario x, we let $x = (x_{ij})_{\langle i,j \rangle \in E} \in \{0, 1\}^{|E|}$ denote the vector of link states. For each link $\langle i, j \rangle \in E$, the binary variable x_{ij} indicates its operational status, where $x_{ij} = 1$ indicates that the link is unavailable (failed), while $x_{ij} = 0$ indicates that it is operational. We consider disruption scenarios with exactly $f \in \mathbb{N}$ failed links. The corresponding combinatorial disruption set is as follows:

$$\mathcal{X} := \Big\{ x \in \{0, 1\}^{|E|} : \sum_{\langle i,j \rangle \in E} x_{ij} = f \Big\}. \tag{3.1}$$

As stated earlier, we let y denote the routing variable determined by the SCN when adapting to a failure scenario x. Then, if a link fails ($x_{ij} = 1$), its capacity is effectively reduced to zero; otherwise, the full capacity is available. Thus, this effective capacity requirement is modeled as follows:

$$y_{ij} \leq (1 - x_{ij}) c_{ij}, \quad \forall \langle i, j \rangle \in E, \tag{3.2}$$

where y_{ij} for every link $\langle i, j \rangle \in E$ denotes the total flow routed on link $\langle i, j \rangle$.

Flow feasibility: For a given disruption scenario x, feasible flows y must satisfy the capacity constraints (3.2) and flow balance constraints. The retailer demand balance constraint is given by the following:

$$\sum_{\substack{w\in W:\\ \langle w,r\rangle\in E}} y_{wr} = D_r - d_r, \quad \forall r \in R, \tag{3.3}$$

where $d_r \geq 0$ is the variable unmet demand for retailer $r \in R$. Flow conservation at intermediate nodes is enforced as follows:

$$\sum_{s\in S:\langle s,p\rangle\in E} y_{sp} = \sum_{w\in W:\langle p,w\rangle\in E} y_{pw}, \quad \forall p \in P, \tag{3.4}$$

$$\sum_{p\in P:\langle p,w\rangle\in E} y_{pw} = \sum_{r\in R:\langle w,r\rangle\in E} y_{wr}, \quad \forall w \in W. \tag{3.5}$$

Constraints in (3.4) and (3.5) model the fact that the total flow arriving into a node i is equal to the total flow leaving i, where $i \in P \cup W$. Given a disruption scenario x, we hereafter refer to the set of constraints in {(3.2), (3.3), (3.4), (3.5), $d \geq 0$, and $y \geq 0$} as the *flow constraints*.

Performance measures: The service performance is measured using the TLD across all retailers, and we model it as TLD = $\sum_{r\in R} d_r$. TLD provides a direct measure of service degradation and is widely used in disrupted supply chain settings (for instance, see [36, 37]). From a managerial perspective, it captures unmet customer demand and directly relates to lost sales and customer dissatisfaction. For each link $\langle i, j\rangle \in E$, let m_{ij} denote its transportation mode, ℓ_{ij} denote its transportation distance in miles, and $\rho^{m_{ij}}$ denote the mode specific freight emission factor. We define the link specific emission coefficient as follows:

$$\eta_{ij} = \rho^{m_{ij}} \ell_{ij}. \tag{3.6}$$

Accordingly, if flow is measured in short tons and $\rho^{m_{ij}}$ is measured in kg CO_2 per short-ton-mile, then $\eta_{ij} y_{ij}$ represents the kg CO_2 generated by transporting flow y_{ij} on link $\langle i, j\rangle$. Accordingly, the TCE represents the total transportation-related carbon emissions associated with a routing y and is given by the following:

$$\text{TCE} = \sum_{\langle i,j\rangle\in E} \rho^{m_{ij}} \ell_{ij} y_{ij} = \sum_{\langle i,j\rangle\in E} \eta_{ij} y_{ij}. \tag{3.7}$$

3.1. Service–carbon tradeoff formulation

For a given disruption scenario x with f failed links satisfying (3.1), we analyze the tradeoff between the TLD and the TCE using an ϵ-constraint approach. We impose an upper limit ϵ on the TCE and determine the minimum achievable TLD under this limit. For a fixed value of ϵ, the first stage problem is as follows:

$$z^*(x, \epsilon) = \min_{y,d} \Big\{ \text{TLD} \;\Big|\; \text{flow constraints}, \sum_{\langle i,j\rangle\in E} \eta_{ij} y_{ij} \leq \epsilon \Big\}, \tag{3.8}$$

where TLD = $\sum_{r\in R} d_r$. Thus, $z^*(x, \epsilon)$ represents the minimum TLD achievable under the disruption scenario x when the TCE is restricted to be no greater than ϵ. Problem (3.8) minimizes the TLD but does not distinguish among alternative routing solutions that attain the same optimal TLD. Consequently, if multiple TLD optimal solutions exist, then they may have different levels of transportation-related carbon emissions. To ensure that the reported service–carbon point does not contain unnecessary emissions, we employ a lexicographic optimization procedure. After obtaining $z^*(x, \epsilon)$ from (3.8), we solve the following second stage problem:

$$\mathrm{TCE}^*(x,\epsilon)=\min_{y,d}\Big\{\sum_{\langle i,j\rangle\in E}\eta_{ij}y_{ij}\;\Big|\;\text{flow constraints},\sum_{\langle i,j\rangle\in E}\eta_{ij}y_{ij}\le\epsilon,\sum_{r\in R}d_r=z^*(x,\epsilon)\Big\}. \tag{3.9}$$

Hence, the first stage minimizes the TLD under the prescribed emission limit, while the second stage minimizes the TCE among all routing solutions that attain the optimal TLD from the first stage. Therefore, the resulting service–carbon point associated with ϵ is defined as $(\mathrm{TCE}_\epsilon, \mathrm{TLD}_\epsilon) = (\mathrm{TCE}^*(x,\epsilon), z^*(x,\epsilon))$. By varying ϵ, the lexicographic procedure generates the service–carbon tradeoff, where ϵ is an upper limit on the TCE. Increasing ϵ expands the feasible routing set, while the second stage optimization selects the minimum TCE solution among all solutions attaining the optimal TLD for that ϵ. Thus, the procedure eliminates unnecessary emissions without altering the optimal service level.

Modeling scope: The model focuses on the operational tradeoff between service and transportation-related carbon emissions. The TCE only includes emissions generated by transportation flows on the modeled network links; emissions associated with production, facilities, inventory holding, or other supply chain activities are not included. The parameter ϵ is an emission limit, not a monetary budget. The transportation cost, lead time, and other operational constraints are outside the present scope; therefore, the model feasibility does not imply financial or temporal feasibility in a specific real world setting.

Structural properties of the service–carbon value function: For a fixed disruption scenario x, define the service–carbon value function $V_x(\epsilon) := z^*(x,\epsilon)$, where $z^*(x,\epsilon)$ is given by (3.8). Some qualitative properties of $V_x(\epsilon)$ directly follows from the optimization structure.

Proposition 1. *For a fixed scenario x and any two emission limits $0 \le \epsilon_1 \le \epsilon_2$, we have $V_x(\epsilon_2) \le V_x(\epsilon_1)$.*

Proof. Let $\mathcal{F}(x,\epsilon)$ denote the feasible set of (3.8). Since $\epsilon_1 \le \epsilon_2$, every solution satisfying the emission constraint at ϵ_1 also satisfies it at ϵ_2. Hence, $\mathcal{F}(x,\epsilon_1) \subseteq \mathcal{F}(x,\epsilon_2)$. Because the same TLD objective is minimized over these two sets, minimization over the larger feasible set cannot produce a larger optimal value. Therefore, $V_x(\epsilon_2) \le V_x(\epsilon_1)$. □

Proposition 2. *Consider two disruption scenarios $x^{(1)}, x^{(2)} \in \{0,1\}^{|E|}$ such that $x^{(1)}_{ij} \le x^{(2)}_{ij}$ for every $\langle i,j\rangle \in E$. Then, for every emission limit $\epsilon \ge 0$, $V_{x^{(2)}}(\epsilon) \ge V_{x^{(1)}}(\epsilon)$. Thus, when a disruption scenario is obtained from another solely by failing additional links, the minimum achievable TLD cannot improve.*

Proof. Under $x^{(2)}$, the available capacity of every link is no greater than under $x^{(1)}$. Consequently, for any fixed ϵ, every routing solution feasible under $x^{(2)}$ is also feasible under $x^{(1)}$. Therefore, $\mathcal{F}(x^{(2)},\epsilon) \subseteq \mathcal{F}(x^{(1)},\epsilon)$. Minimizing TLD over the smaller feasible set cannot yield a lower optimal value, which establishes the result. □

Therefore, the nontrivial question examined in the remainder of the paper is *how much* service improvement is obtained as the emission limit is relaxed, how marginal recovery efficiency changes along the frontier, and how disruption severity and network structure affect the resulting marginal improvement profiles. These effects are captured by the shape of the lexicographically efficient frontier and by the marginal improvement measure in Sections 4 and 5.

3.2. Carbon-emission limit range

As stated earlier, for a given disruption scenario x, the service–carbon frontier is evaluated over a range of emission limits ϵ. The lower endpoint is set to zero. The upper endpoint, denoted by $\epsilon_{\mathrm{Max}}(x)$, is defined as the minimum level of TCE required to attain the best achievable service performance under scenario x. To determine this value, we first solve the TLD minimization problem without imposing a transportation-related carbon emission constraint:

$$z_{\min}(x) = \min_{y,d} \{\text{TLD} \mid \text{flow constraints}\}. \tag{3.10}$$

The value $z_{\min}(x)$ represents the minimum TLD attainable under disruption scenario x when no restriction is imposed on the TCE. Therefore, we interpret $z_{\min}(x)$ as a *carbon unconstrained service recovery benchmark*: it represents a service prioritizing recovery policy that minimizes unmet demand without imposing an environmental restriction on the routing response. This provides a natural carbon agnostic benchmark against which the service outcomes obtained under finite emission limits can be compared. Because multiple routing solutions may attain $z_{\min}(x)$ while producing different emission levels, using the TCE of an arbitrary TLD optimal routing would make the upper endpoint dependent on the particular optimal solution returned by the solver. Therefore, we apply a second lexicographic optimization and define the following:

$$\epsilon_{\mathrm{Max}}(x) = \min_{y,d} \Big\{ \sum_{\langle i,j\rangle \in E} \eta_{ij} y_{ij} \;\Big|\; \text{flow constraints}, \sum_{r\in R} d_r = z_{\min}(x) \Big\}. \tag{3.11}$$

Thus, $\epsilon_{\mathrm{Max}}(x)$ is the minimum TCE required to attain the carbon unconstrained benchmark $z_{\min}(x)$. Consequently, $z^*(x, \epsilon_{\mathrm{Max}}(x)) = z_{\min}(x)$, and increasing the emission limit beyond $\epsilon_{\mathrm{Max}}(x)$ cannot further reduce the TLD. Therefore, the endpoint $\epsilon = \epsilon_{\mathrm{Max}}(x)$ represents the service prioritizing carbon unconstrained recovery benchmark on the service–carbon frontier. Accordingly, the service–carbon frontier is evaluated over $\epsilon \in [0, \epsilon_{\mathrm{Max}}(x)]$. For the computational experiments, the interval $[0, \epsilon_{\mathrm{Max}}(x)]$ is discretized using a normalized uniform grid of 101 emission limit levels. Specifically, we define the following:

$$\epsilon_k(x) = \frac{k}{100}\epsilon_{\mathrm{Max}}(x), \qquad k = 0, 1, \ldots, 100. \tag{3.12}$$

Thus, consecutive emission limits differ by $0.01\,\epsilon_{\mathrm{Max}}(x)$, and the grid spans the relevant emission limit interval from zero to the minimum emission level required to attain the best achievable service performance. Normalizing the grid by $\epsilon_{\mathrm{Max}}(x)$ provides a consistent relative resolution across disruption scenarios and network instances whose absolute emission ranges may differ.

3.3. Disruption scenario selection

Our objective is to characterize how the service–carbon tradeoff evolves as the emission limit ϵ varies for a *fixed* disrupted network. This isolates the effect of changing the allowable emissions from the effect of changing the underlying failed link configuration. For the principal computational experiments, we select a fixed adverse benchmark scenario using a network interdiction criterion based on an unconstrained service performance. For a prescribed number $f \in \mathbb{N}$ of failed links, we use $\mathcal{X}$ defined in (3.1). For any $x \in \mathcal{X}$, the network optimally responds by rerouting the flow so as to minimize the TLD. Therefore, the adverse disruption scenario x^* is defined by solving the following:

$$\Phi_f = \max_{x \in \mathcal{X}} \min_{y,d} \Big\{ \sum_{r \in R} d_r \;\Big|\; \text{flow constraints} \Big\}, \tag{3.13}$$

where x^* denotes an optimal disruption scenario attaining (3.13). The inner minimization problem is a linear program (LP) for every fixed x; we replace it by its LP dual. Let α, γ, θ, and λ be as defined in Table 2; then, by strong duality, (3.13) is equivalently written as the following single level problem:

$$\Phi_f = \max_{x,\alpha,\gamma,\theta,\lambda} \quad \sum_{r \in R} D_r \lambda_r - \sum_{\langle i,j \rangle \in E} c_{ij} \alpha_{ij} (1 - x_{ij}) \tag{3.14}$$

$$\text{s.t.} \quad \gamma_p - \alpha_{sp} \le 0, \qquad \forall \langle s, p \rangle \in E_{SP}, \tag{3.15}$$

$$\theta_w - \alpha_{pw} - \gamma_p \le 0, \qquad \forall \langle p, w \rangle \in E_{PW}, \tag{3.16}$$

$$\lambda_r - \alpha_{wr} - \theta_w \le 0, \qquad \forall \langle w, r \rangle \in E_{WR}, \tag{3.17}$$

$$\alpha \ge 0, \;\; \lambda \le 1, \tag{3.18}$$

$$x \in \{0, 1\}^{|E|}, \;\; \sum_{\langle i,j \rangle \in E} x_{ij} = f. \tag{3.19}$$

This disruption criterion identifies x^* as the most damaging scenario in $\mathcal{X}$ in terms of the optimally recovered service when no transportation-related carbon emission restriction is imposed. Once selected, x^* is held fixed while ϵ is varied. Therefore, the selected scenario is not asserted to be the pointwise worst disruption for every individual value of ϵ. As the framework itself is applicable to any fixed disruption scenario, we additionally examine the sensitivity of the computational findings to different scenario selection rules in Sections 4 and 5.

Computational implementation: The problem in (3.14)–(3.19) is solved as a nonconvex mixed-integer bilinear model using Gurobi's global optimization procedure for nonconvex quadratic/bilinear formulations. All such disruption selection instances used in the reported experiments were solved to proven optimality. To assess the computational behavior of the disruption selection formulation as the network size increases, we additionally solve five four-echelon instances of increasing size while fixing the link generation probability at $p = 0.5$ and the failure budget at $f = 3$. Table 3 reports the resulting runtime and final optimality gap.

Table 3. Solving (3.14) – (3.19) for increasing SCN sizes ($p = 0.5$, $f = 3$).

$(\lvert S \rvert, \lvert P \rvert, \lvert W \rvert, \lvert R \rvert)$	$\lvert V \rvert$	$\lvert E \rvert$	Runtime (s)	MIP gap
(4, 4, 4, 8)	20	31	0.220	0
(6, 5, 5, 8)	24	47	0.399	0
(8, 7, 6, 14)	35	95	2.639	0
(8, 9, 6, 12)	35	125	3.216	0
(10, 10, 12, 16)	48	209	113.652	0

Table 3 shows the increasing computational effort as network size grows. Instances with 95 and 125 links are solved in approximately 2.64 and 3.22 seconds, respectively, whereas the largest tested instance, with 209 links, requires approximately 113.65 seconds. All five instances terminate with a zero final optimality gap.

3.4. *Pareto frontier computation*

The service–carbon frontier is constructed by applying the lexicographic procedure in (3.8)–(3.9) for a sequence of transportation-related carbon emission limits as in (3.12). For each ϵ, the first stage problem determines the minimum achievable TLD, and the second stage problem identifies the minimum TCE routing among all solutions attaining that TLD. Therefore, the resulting pair $(\mathrm{TCE}_\epsilon, \mathrm{TLD}_\epsilon)$ represents the lexicographically efficient operating point associated with ϵ. The procedure used to construct the frontier is summarized in Algorithm 1.

Algorithm 1 Obtaining the service–carbon frontier $\mathcal{P} = \{(\mathrm{TCE}_k, \mathrm{TLD}_k)\}_k$

Input: SCN (V, E); Fixed disruption scenario x.
Output: Service–carbon frontier $\mathcal{P}$ between TCE and TLD.
Solve (3.10) for x to obtain $z_{\min}(x)$
Solve (3.11) with $\sum_{r\in R} d_r = z_{\min}(x)$ to obtain $\epsilon_{\mathrm{Max}}(x)$
Generate the normalized emission limit grid $\epsilon_k(x) = \dfrac{k}{100}\epsilon_{\mathrm{Max}}(x), \quad k = 0, \ldots, 100$ as in (3.12)
for $k = 0, \ldots, 100$ **do**
    Solve (3.8) with $\epsilon = \epsilon_k(x)$ to obtain $\mathrm{TLD}_k = z^*(x, \epsilon_k)$
    Solve (3.9) with $\sum_{r\in R} d_r = \mathrm{TLD}_k$ to obtain $\mathrm{TCE}_k = \mathrm{TCE}^*(x, \epsilon_k)$
    Record the lexicographically efficient solution pair $(\mathrm{TCE}_k, \mathrm{TLD}_k)$
end for
Construct the service–carbon frontier $\mathcal{P} = \{(\mathrm{TCE}_k, \mathrm{TLD}_k)\}_k$

4. Experimental Design

To evaluate the proposed framework, we generate synthetic multi echelon SCN instances that capture the key operational characteristics of real world logistics systems. The generation procedure is designed to reflect the structural, operational, and environmental aspects of supply chains, including multi stage flows, heterogeneous transportation modes, and capacity driven routing decisions. A summary of the primary experimental setup is provided in Table 4.

Table 4. Summary of the primary SCN instance parameters.

Parameter	Value
$(\|S\|, \|P\|, \|W\|, \|R\|)$	(8, 7, 6, 14)
Number of failed links in SCN	$f \in \{0, 1, 2, 3, 5\}$
Connectivity screening	Retailers reachable; intermediate nodes active
Demand range	$\mathcal{U}[60, 100]$ short-ton
Rail, Road, Air capacity	$\mathcal{U}[35, 50], \mathcal{U}[20, 35], \mathcal{U}[8, 18]$ short-ton
Transportation-mode probabilities	(0.50, 0.35, 0.15) for rail, road, and air
Transportation distance ℓ_{ij} (miles)	$\mathcal{U}[100, 1000]$
Emission factors $(\rho^{\mathrm{rail}}, \rho^{\mathrm{road}}, \rho^{\mathrm{air}})$	(0.021, 0.210, 1.461) kg CO_2/short-ton-mile [38]

Network generation: We consider a four-echelon SCN, where connectivity between consecutive echelons is generated using random bipartite graphs for *link probability p*. To prevent a nominal network performance from being driven by structural disconnection, the constructed SCN is screened before it is accepted for experiments. An instance is retained only if:

(A1) Connectivity screening: Every $r \in R$ is reachable from at least one $s \in S$ through a path S to P to W to R; every $p \in P$ has at least one incoming supplier link and at least one outgoing warehouse link; and every $w \in W$ has at least one incoming plant link and at least one outgoing retailer link.

In Table 4, we refer to these three conditions as *connectivity screening*. Each link is assigned a transportation mode from $\{\text{rail}, \text{road}, \text{air}\}$ with probabilities $(0.50, 0.35, 0.15)$, respectively. The transportation mode is treated as a fixed link attribute rather than as an endogenous mode switching decision. To provide an interpretable physical basis for the carbon emission measure, each link is also assigned a transportation distance of $\ell_{ij} \sim \mathcal{U}[100, 1000]$ miles. The mode specific freight emission factors are set to $(\rho^{\text{rail}}, \rho^{\text{road}}, \rho^{\text{air}}) = (0.021, 0.210, 1.461)$ kg CO_2 per short-ton-mile, based on the illustrative U.S. modal average freight emission factors reported by the U.S. Environmental Protection Agency's SmartWay program [38]. The resulting link specific emission coefficient is $\eta_{ij} = \rho^{m_{ij}} \ell_{ij}$, as defined in (3.6). Hence, the TCE jointly accounts for the transportation mode, distance, and routed flow.

Capacity and demand generation: The link capacities are generated as mode dependent random variables. Specifically, each link $\langle i, j \rangle \in E$ is assigned a capacity c_{ij} drawn from a uniform distribution based on its transportation mode: rail links from $[35, 50]$, road links from $[20, 35]$, and air links from $[8, 18]$. Demand is generated at the retail level. Each retailer demand is independently sampled from a uniform distribution $D_r \sim \mathcal{U}[60, 100]$ for every $r \in R$. The demand and capacity ranges are deliberately calibrated to create capacity-stressed SCNs in which the transportation capacity is under substantial pressure relative to the demand. This setting is intended to represent operating conditions that can arise during periods of elevated demand, constrained transportation capacity, congestion, or other operational strain. Such conditions are particularly relevant to study disruption and recovery because subsequent link failures occur when the residual capacity is already limited, making the effects of routing flexibility, capacity loss, and emission restrictions on the service recovery operationally consequential.

Computation of Pareto front: We compute the service–carbon frontier using Algorithm 1. While the Pareto frontier captures the set of efficient operating points, additional metrics are required to interpret its structure and the effectiveness of recovery strategies. To this end, we compute two complementary measures. First, we evaluate the *service level %*, which is defined as follows:

$$L_k = \frac{\text{Total Demand} - \text{TLD}_k}{\text{Total Demand}} \times 100, \tag{4.1}$$

which provides a normalized measure of system performance. This facilitates a comparison across network realizations and network sizes with different total demand. Second, we compute the *marginal improvement* in service with respect to the TCE between consecutive lexicographically efficient frontier points. For consecutive points $k-1$ and k, this measure is defined as follows:

$$M_k = -\frac{\text{TLD}_k - \text{TLD}_{k-1}}{\text{TCE}_k - \text{TCE}_{k-1}}, \tag{4.2}$$

whenever $\text{TCE}_k > \text{TCE}_{k-1}$. Therefore, the measure represents the reduction in lost demand obtained per additional unit of the TCE between consecutive distinct frontier points. Larger values indicate greater service improvements per unit of additional emissions, whereas smaller values indicate diminishing marginal improvements. Before computing M_k, consecutive frontier points with identical TCE values, up to the numerical tolerance used in the computations, are removed so that the denominator in (4.2) is strictly positive. The marginal improvement measure is directly evaluated between consecutive distinct efficient points. Changes in the level of M_k are descriptively used to characterize regions of relatively higher or lower marginal improvement. We do not impose a formal breakpoint detection rule; therefore, references to such regions and transitions describe features of the marginal improvement profiles rather than uniquely identified structural breakpoints. Together, these three representations:

(A2) TLD versus TCE; Service level % versus TCE; Marginal improvement versus TCE,

provide a comprehensive view of the tradeoff. The first characterizes the attainable performance boundary, the second normalizes performance for comparability, and the third reveals the marginal service improvement associated with an additional TCE across different portions of the tradeoff.

Computational implementation: All optimization models are implemented in Python and solved using the Gurobi Optimizer 13.0.1 [39]. All computations are performed on a machine running Ubuntu 24.04.4 LTS equipped with a 12th Gen Intel(R) Core(TM) i7-1265U processor with 10 physical cores and 12 logical processors.

The computational experiments are organized to examine the robustness of the service–carbon tradeoff along several dimensions of the experimental setting. First, we vary the underlying SCN structure through the network density, topology, and network size. Then, we examine the sensitivity to the freight emission factors, retailer demand, and transportation mode composition. Finally, we assess whether the observed service–carbon patterns depend on the rule used to select the fixed disruption scenario. Unless otherwise stated, the principal max–min disruption selection criterion in (3.13) and the experimental parameters in Table 4 are used.

4.1. Varying the underlying structural network

First, we examine the sensitivity of the service–carbon tradeoff to three structural characteristics of the SCN: link density, connectivity topology, and network size. For the replicated experiments, the results are aligned by the normalized emission-limit level $\epsilon/\epsilon_{\text{Max}}$. At each common normalized level, the TCE, TLD, and service level are separately averaged across the independent network realizations, yielding mean tradeoff points $(\overline{\text{TCE}}, \overline{\text{TLD}})$ and the corresponding mean service levels. Although each realization-specific (TCE, TLD) pair is a feasible lexicographically efficient operating point for that realization, a pair $(\overline{\text{TCE}}, \overline{\text{TLD}})$ obtained by separately averaging the two coordinates across realizations need not itself correspond to a feasible operating point of any individual network. Accordingly, the resulting mean curves are interpreted as descriptive cross-realization service–carbon tradeoff profiles rather than Pareto frontiers. The 95% confidence interval for a reported mean is computed as $\bar{z} \pm t_{0.975,n-1}\frac{s}{\sqrt{n}}$, where $\bar{z}$ and s denote the sample mean and sample standard deviation, respectively, and n is the number of independent realizations. For marginal improvement summaries, n at a given interval denotes the number of realizations with a strictly positive TCE increment for that interval.

4.1.1. Varying SCN link density by changing link probability p

We evaluate the service carbon frontier using the representations stated in Item (A2) for different link probability values:

(A3) $p = 0.4$ (sparse network); $p = 0.5$ (moderate network); $p = 0.6$ (dense network).

These values allow us to study how network connectivity influences the routing flexibility and resilience under disruption. To isolate the effect of the network density from incidental differences in random topology, the three density levels are generated using a nested common random number construction. Specifically, each potential link $\langle i, j\rangle$ is assigned a single independent draw $u_{ij} \sim \mathcal{U}[0, 1]$, and the link is included in the network at density p whenever $u_{ij} < p$. Consequently, $E(0.4) \subseteq E(0.5) \subseteq E(0.6)$, where E represents the edge set. For the nested density experiment, the mode, capacity, distance, and the resulting emission coefficient are generated once for each potential link and retained whenever that link appears at multiple density levels. Consequently, increasing the network density adds links without changing the physical attributes of links already present. This construction allows the density comparison to reflect an increased connectivity rather than uncontrolled differences between independently generated networks. To prevent a nominal network performance from being driven by structural disconnection, the sparsest network, $E(0.4)$, is screened as per (A1) before the nested family is accepted. This works as the density levels are nested, and satisfaction of these conditions by $E(0.4)$ implies that they also hold for $E(0.5)$ and $E(0.6)$. If these conditions are not satisfied, then a new common random number realization is generated. Thus, positive nominal TLD in the accepted instances is attributable to capacity and routing limitations rather than structurally disconnected retailers or inactive intermediate nodes. Additionally, to characterize the nominal networks independent of the carbon constraint and disruption scenarios, we evaluate each accepted instance with no failed links and without an emission constraint. Table 5 reports the resulting structural and capacity diagnostics. The maximum deliverable flow is obtained by minimizing the TLD in the nominal network, so that $\text{Flow}_{\max} = \sum_{r\in R} D_r - \text{TLD}_{\text{nom}}$.

Table 5. Nominal SCN capacity and bottleneck diagnostics across ten independent network realizations $(|S|, |P|, |W|, |R|) = (8, 7, 6, 14)$.

p	$\lvert E\rvert$	$\sum_{E_{SP}} c_{ij}$	$\sum_{E_{PW}} c_{ij}$	$\sum_{E_{WR}} c_{ij}$	$\text{Flow}_{\max}$	TLD_{nom}	Service (%)
0.4	71.40 (5.04)	772.53 (134.81)	488.68 (70.83)	1057.81 (129.28)	392.10 (57.32)	646.15 (57.32)	37.77 (5.52)
0.5	89.30 (7.73)	949.61 (184.67)	630.43 (47.42)	1336.27 (128.02)	535.32 (61.84)	502.92 (61.84)	51.56 (5.96)
0.6	107.50 (8.03)	1113.19 (154.29)	760.05 (90.63)	1613.93 (109.31)	695.45 (82.67)	342.79 (82.67)	66.98 (7.96)

Node-level capacity diagnostics (average minimum / mean / maximum)

p	Plant bottleneck	Warehouse bottleneck	Retailer incoming capacity
0.4	19.82 / 58.17 / 106.80	35.39 / 77.73 / 124.01	22.98 / 75.56 / 149.89
0.5	32.70 / 78.16 / 130.60	46.91 / 100.50 / 150.76	27.57 / 95.45 / 167.04
0.6	55.23 / 99.99 / 153.65	70.62 / 125.92 / 182.53	48.27 / 115.28 / 186.30

Values are mean (standard deviation) across 10 nested network realizations; node level entries report average minimum / mean / maximum. For P and W, node capacity is the minimum of total incoming and outgoing capacity; for R, it is total incoming capacity. All realizations satisfy (A1). Capacities and flows are in short tons.

The diagnostics in Table 5 confirm that the accepted nested instances are structurally viable before disruptions are introduced. At all three density levels, the aggregate $P \to W$ capacity is the smallest of the three echelon capacities, indicating that the plant to warehouse stage has the tightest aggregate capacity among the three echelons. The node level diagnostics further show substantial heterogeneity in the available capacity across plants, warehouses, and retailers even though all nodes satisfy the structural screening conditions. The resulting nominal service levels of 37.77%–66.98% should be interpreted in the context of this capacity-stressed calibration. Here, "nominal" denotes the absence of modeled link failures ($f = 0$), rather than an unconstrained SCN with an abundant spare capacity. Thus, the positive nominal TLD reflects an SCN already operating under capacity pressure before additional link failures are introduced. Therefore, the reported service levels are outcomes of the stressed synthetic experimental setting and are not intended as universal service-level benchmarks for real-world SCNs. As network density increases, the nominal TLD decreases and nominal service increases. Using the SCN structure in Table 4, we evaluate $p \in \{0.4, 0.5, 0.6\}$ and $f \in \{0, 1, 2, 3, 5\}$, with disruption scenarios selected by (3.13). The experiment is repeated over ten independent network realizations, and each service–carbon frontier is evaluated using the 101 emission limit levels in (3.12). The resulting service–carbon tradeoffs are shown in Figure 1.

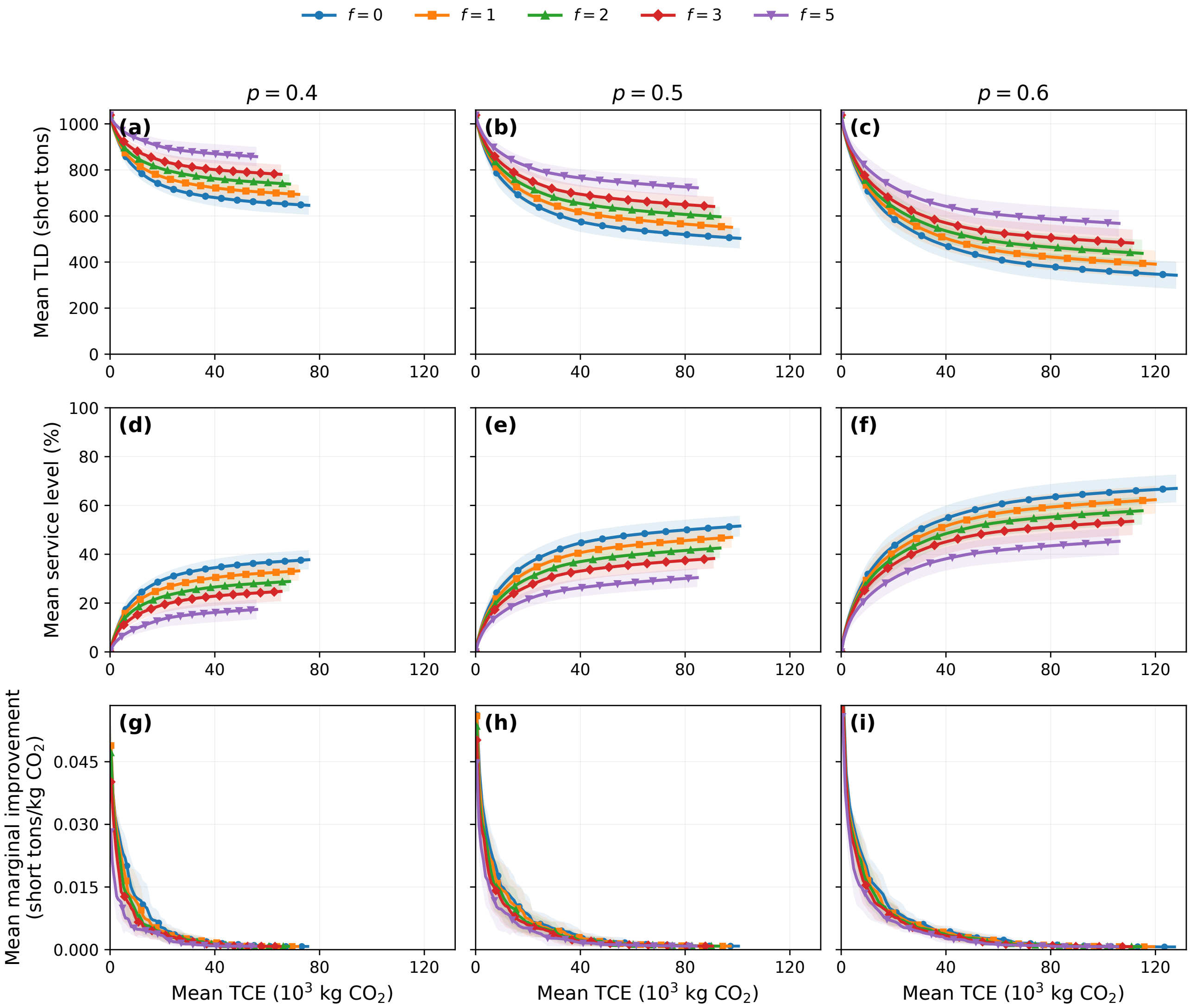

Figure 1. Mean service–carbon tradeoffs across network densities $p \in \{0.4, 0.5, 0.6\}$ and disruption levels $f \in \{0, 1, 2, 3, 5\}$, with 95% confidence intervals.

4.1.2. Varying SCN structural topology

To examine the robustness of the service–carbon findings to network structure, we conduct a controlled topology experiment using three four-echelon structures:

(A4) random layered, hub-dominated layered, and degree-balanced redundant topologies.

All structures preserve the directed $S \to P \to W \to R$ architecture and satisfy (A1). For each $p \in \{0.4, 0.5, 0.6\}$ and within each controlled realization, the three topology classes have identical node sets and echelon-specific link counts and use the same within echelon multisets of transportation modes, capacities, distances, and emission coefficients, which are generated as described in Table 4. Thus, the topology primarily differ in how the connectivity is distributed across intermediate nodes. The hub-dominated topology concentrates links around selected plants and warehouses, the degree-balanced topology distributes links more evenly, and the random topology provides the benchmark. Operationally, the hub-dominated topology is generated by assigning higher selection scores to links incident to designated plant and warehouse hubs, whereas the degree-balanced topology is greedily generated by favoring links whose endpoints currently have the lowest combined degree. In all cases, the prescribed echelon-specific link counts are preserved. We characterize these structural differences using the coefficient of variation (CV) of intermediate node total degree, defined as the sum of incoming and outgoing link counts, and the share of total intermediate node degree associated with the two highest degree nodes. Table 6 reports these diagnostics for the representative $p = 0.5$ case. For each topology and p, we evaluate $f \in \{0, 1, 2, 3, 5\}$ using the max–min disruption scenario from (3.13). The experiment is repeated over ten controlled network realizations, and each service–carbon frontier is evaluated using the 101 emission limit levels in (3.12). The results are reported in Section 5.2.

Table 6. Structural diagnostics for topology classes at $p = 0.5$ across ten controlled network realizations; $(|S|, |P|, |W|, |R|) = (8, 7, 6, 14)$.

Topology	Degree CV	Min deg.	Max deg.	Top-2 share	$\|E\|$
Random	0.308 (0.023)	4.40 (1.52)	13.00 (0.71)	0.223 (0.009)	91
Hub-dominated	0.752 (0.004)	3.20 (0.45)	21.00 (0.00)	0.371 (0.005)	91
Degree-balanced	0.215 (0.000)	7.00 (0.00)	11.00 (0.00)	0.196 (0.000)	91

Values are mean (standard deviation). Within each realization, topology classes share identical echelon-specific link counts, $(|E_{SP}|, |E_{PW}|, |E_{WR}|) = (28, 21, 42)$, and within-echelon multisets of modes, capacities, distances, and emission coefficients.

4.1.3. Varying the sizes for $|S|, |P|, |W|$, and $|R|$

In addition to the primary SCN size reported in Table 4, we examine three network sizes: $(|S|, |P|, |W|, |R|) = (6, 5, 5, 8)$, $(8, 9, 6, 12)$, and $(10, 10, 12, 16)$. For each size, we consider $p \in \{0.4, 0.5, 0.6\}$ using the nested network construction described in Section 4.1.1, while the remaining parameters are generated as specified in Table 4. For each network, disruption scenarios are constructed for $f \in \{0, 1, 2, 3, 5\}$ by solving (3.13). The experiment is repeated over ten independent network realizations, and each service–carbon frontier is evaluated using the 101 emission limit levels in (3.12). The results are reported in Section 5.3.

4.2. Varying emission factors, retailer demands, and transportation mode composition

Using the primary SCN parameters in Table 4, we conduct a sensitivity analysis on the representative random layered network with $p = 0.5$ by varying the freight emission factors, retailer demand, and transportation mode composition. Unless otherwise stated, the remaining network parameters are held at their baseline values. For the emission factors, the EPA-based baseline

$(0.021, 0.210, 1.461)$ kg CO_2 per short-ton-mile is compared with lower contrast $(0.021, 0.150, 0.900)$ and higher contrast $(0.021, 0.300, 2.000)$ specifications. These are controlled sensitivity cases rather than alternative empirical estimates; topology, modes, distances, capacities, and demands remain fixed. For demand, all retailer demands are uniformly scaled to $0.8D$, D, and $1.2D$, with the network and link attributes unchanged. For the mode composition, the realized baseline rail/road/air shares $(0.516, 0.379, 0.105)$ in the representative network are compared with rail heavy $(0.747, 0.211, 0.042)$ and road/air heavy $(0.232, 0.600, 0.168)$ cases, while the topology and distances remain fixed. Links retaining their mode keep their baseline capacities; reassigned links are mapped to the corresponding mode specific capacity range using the same underlying random quantile. For each sensitivity case, disruption scenarios are selected using (3.13) for $f \in \{0, 1, 2, 3, 5\}$, and the service–carbon tradeoff is evaluated at $\epsilon/\epsilon_{\text{Max}} \in \{0, 0.25, 0.50, 0.75, 1.00\}$. The results are reported in Table 7.

4.3. *Varying selection rule for failure scenario $x \in \mathcal{X}$*

SCN disruptions are modeled by (3.1), with $f \in \{0, 1, 2, 3, 5\}$. In the principal analysis, the fixed disruption scenario for each f is selected using (3.13). To assess the sensitivity to this selection rule, we repeat the frontier analysis using the primary SCN structure in Table 4 and three alternative scenario constructions: (i) under the *critical-link* construction, each link is evaluated according to the minimum TLD obtained when that link alone is failed, and the f links associated with the largest individual TLD values are selected; (ii) under the *random* construction, f links are sampled uniformly without replacement from the set of network links using a fixed random seed; (iii) and finally, under the *representative average random* construction, 30 random f-link disruption scenarios are generated and their minimum unconstrained TLD values are computed, where the actual sampled scenario whose TLD is closest to the mean TLD across the 30 scenarios is selected as the fixed representative scenario. For each scenario selection rule, the experiment is repeated over ten independent network realizations, and each service–carbon frontier is evaluated using the 101 emission limit levels in (3.12). The results are reported in Section 5.5.

5. Results and Discussion

This section presents the computational results following the experimental design in Section 4. First, we examine the principal service–carbon tradeoff across network densities and disruption levels, including the corresponding service level and marginal improvement behavior. Then, we assess the robustness of these findings to changes in the network topology and size, followed by sensitivity analyses for the emission factors, retailer demand, and transportation mode composition. Finally, we examine alternative disruption scenario selection rules and discuss the managerial implications of the results.

5.1. *Results for varying link probability p (Experiment from Section 4.1.1)*

The principal analysis examines how the network density and disruption severity affect the service–carbon tradeoff under the max–min disruption selection criterion. Figure 1 reports the mean service–carbon tradeoff across 10 independent nested network realizations for $p \in \{0.4, 0.5, 0.6\}$ and $f \in \{0, 1, 2, 3, 5\}$. The first row plots the mean TLD against the mean TCE, the second row plots the mean service level against the mean TCE, and the third row plots the mean marginal improvement, $-\Delta(\text{TLD})/\Delta(\text{TCE})$, against the mean TCE. Shaded regions represent 95% confidence intervals across realizations. Taken together, these nine panels provide a detailed view of how disruptions alter not only the achievable performance, but also the marginal service improvement associated with an additional TCE.

Overall structure of the tradeoff: Consistent with Proposition 1, the mean TLD is nonincreasing as the emission limit is relaxed, with Panels (d)–(f) showing the corresponding increase in the mean service level. More importantly, the mean tradeoff profiles exhibit changes in the slope and marginal recovery efficiency across disruption levels and network densities. Panels (g)–(i) exhibit plateaus separated by downward transitions in marginal improvement. To test whether this pattern results from the ϵ discretization in (3.12), we perform a separate grid-refinement check for the representative $p = 0.5$, $f = 3$ case using 51, 101, 201, and 501 emission limit levels. As Figure 2 shows, the frontier and major patterns in the marginal improvement profile remain stable across the grid resolutions, indicating that the observed stepwise pattern is not solely a consequence of the chosen discretization.

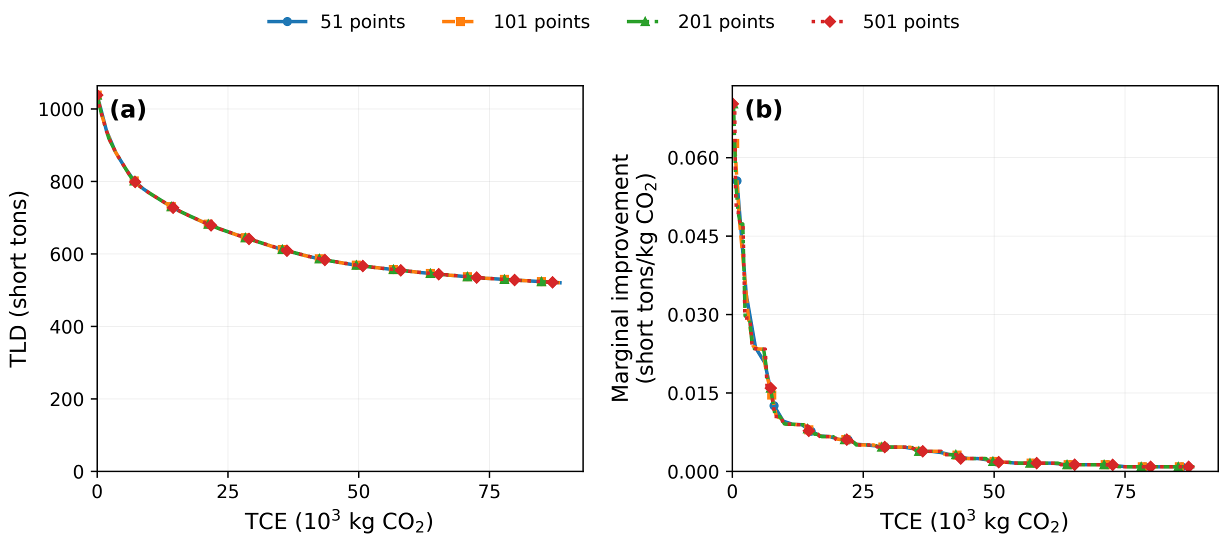

Figure 2. Grid-refinement analysis for $p = 0.5$ and $f = 3$ using 51, 101, 201, and 501 emission limit levels. The TLD–TCE frontier (a) and marginal improvement (b) remain stable across grid resolutions.

TLD–TCE tradeoff across disruption levels: Panels (a)–(c) show the mean tradeoff under the max–min disruption scenarios from (3.13). Across the replicated instances, higher failure budgets shift the mean tradeoff profiles upward, thus yielding higher mean TLD at corresponding normalized emission-limit levels. Because the independently selected scenarios for different f need not be nested, this ordering is specific to the adverse scenario analysis; Section 5.5 examines its robustness under alternative scenario selection criteria. The carbon unconstrained endpoint provides a benchmark to measure the service effect of the emission limit. For $p = 0.5$ and $f = 3$, the mean TLD across the 10 realizations is 641.03 at $\epsilon = \epsilon_{\text{Max}}$, compared with 685.40 at $0.5\,\epsilon_{\text{Max}}$, corresponding to 44.36 additional units of mean lost demand. Thus, the mean tradeoff profile quantifies the average service loss associated with tighter emission limits relative to carbon-unconstrained recovery across the replicated instances. Panels (a)–(c) also flatten as the TCE increases, thus indicating diminishing service gains from progressively relaxing the emission limit.

Effect of network density on attainable performance: Panels (a)–(c) show that increasing the network density from $p = 0.4$ to $p = 0.6$ shifts the mean TLD–TCE tradeoff profile downward across disruption levels, thus indicating lower mean TLD across corresponding normalized emission limit levels. Greater connectivity provides additional routing flexibility, thus improving the nominal performance and recovery under link failures. Denser networks also sustain service improvements over a broader TCE range before the mean tradeoff profile approaches a plateau.

Service level representation: Panels (d)–(f) express the same tradeoff using the mean service level, facilitating comparison across density and disruption levels. The curves approach density- and disruption-dependent service ceilings, showing that relaxing the emission limit cannot fully compensate for disruption induced capacity loss.

Marginal improvement and diminishing returns: Panels (g)–(i) report mean marginal improvements, $-\Delta(\text{TLD})/\Delta(\text{TCE})$, computed within each realization and then averaged across the realizations for which the corresponding TCE increment is strictly positive. The profiles exhibit regions of relatively higher and lower marginal improvements, with smaller service gains generally observed as TCE increases. Larger failure budgets are generally associated with earlier declines toward lower marginal improvement levels, whereas denser networks sustain higher marginal improvements over a broader TCE range. As stated in Section 4, these regions and transitions are interpreted descriptively rather than as formally estimated breakpoints. Attributing individual transitions to specific links, modes, or binding capacities would require a separate active set analysis.

5.2. Robustness across alternative network topologies (Experiment from Section 4.1.2)

Figure 3 shows that the principal service–carbon relationships persist across topology classes and network densities and are therefore not confined to the random layered topology used in the principal experiments. Nevertheless, the topology structure affects the location and extent of the mean tradeoff profiles. For a fixed p, the three topology classes have identical node sets, echelon specific link counts, and link attribute multisets; hence, the observed differences reflect how the controlled link attributes are distributed over different connectivity structures. In the tested instances, the degree balanced topology generally attains a lower TLD than the hub-dominated topology at a comparable TCE, with the random topology often lying between them. These differences show that the distribution of the connectivity can affect the recovery performance even when the network size, density, and aggregate capacity are controlled. Additionally, the absolute TCE range varies with the network density. In particular, the $p = 0.4$ mean tradeoff profiles terminate at lower TCE values and higher TLD levels than the denser cases, indicating earlier exhaustion of carbon enabled recovery opportunities under limited connectivity. Overall, the results support the robustness of the principal service–carbon findings while showing that the network structure materially affects attainable recovery performance.

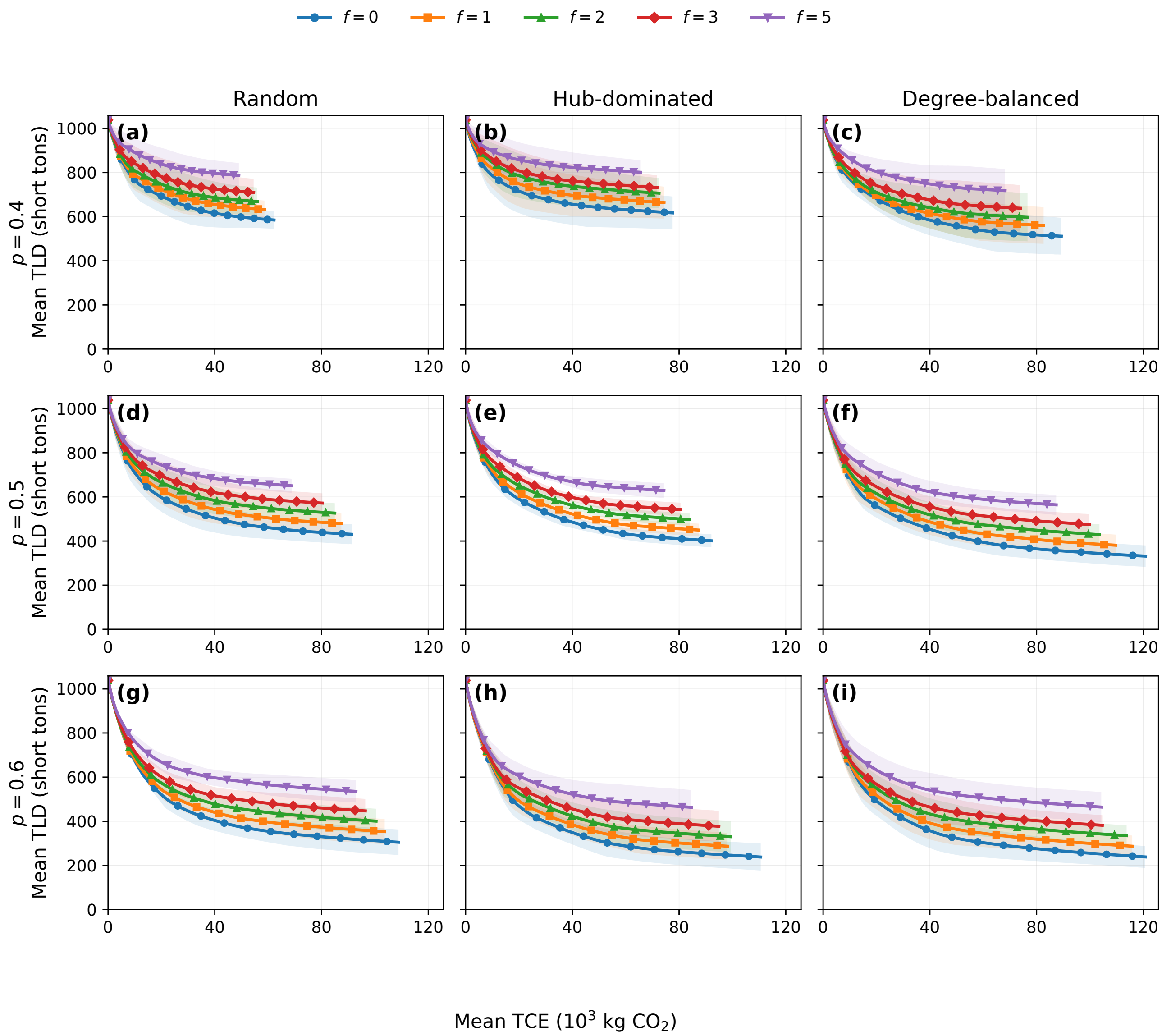

Figure 3. Mean TLD–TCE tradeoff profiles across network densities $p \in \{0.4, 0.5, 0.6\}$ and random, hub-dominated, and degree-balanced topologies, with 95% confidence intervals.

5.3. Robustness across SCN sizes (Experiment from Section 4.1.3)

Figure 4 reports service level rather than absolute TLD because total demand varies with network size; the percentage measure therefore provides a normalized basis for cross size comparison. The principal service–carbon patterns persist across all three sizes: service improves with TCE and generally with network density, while the selected max–min disruptions reduce attainable service.

The f-curves are more separated in the smaller and sparser networks, whereas this separation generally narrows as size and density increase. For the largest network at $p = 0.6$, the curves cluster near full service, indicating that greater routing flexibility mitigates the effect of the selected adverse disruptions. Thus, the qualitative findings persist across the tested SCN sizes, while the magnitude of disruption induced service loss depends on network size and connectivity.

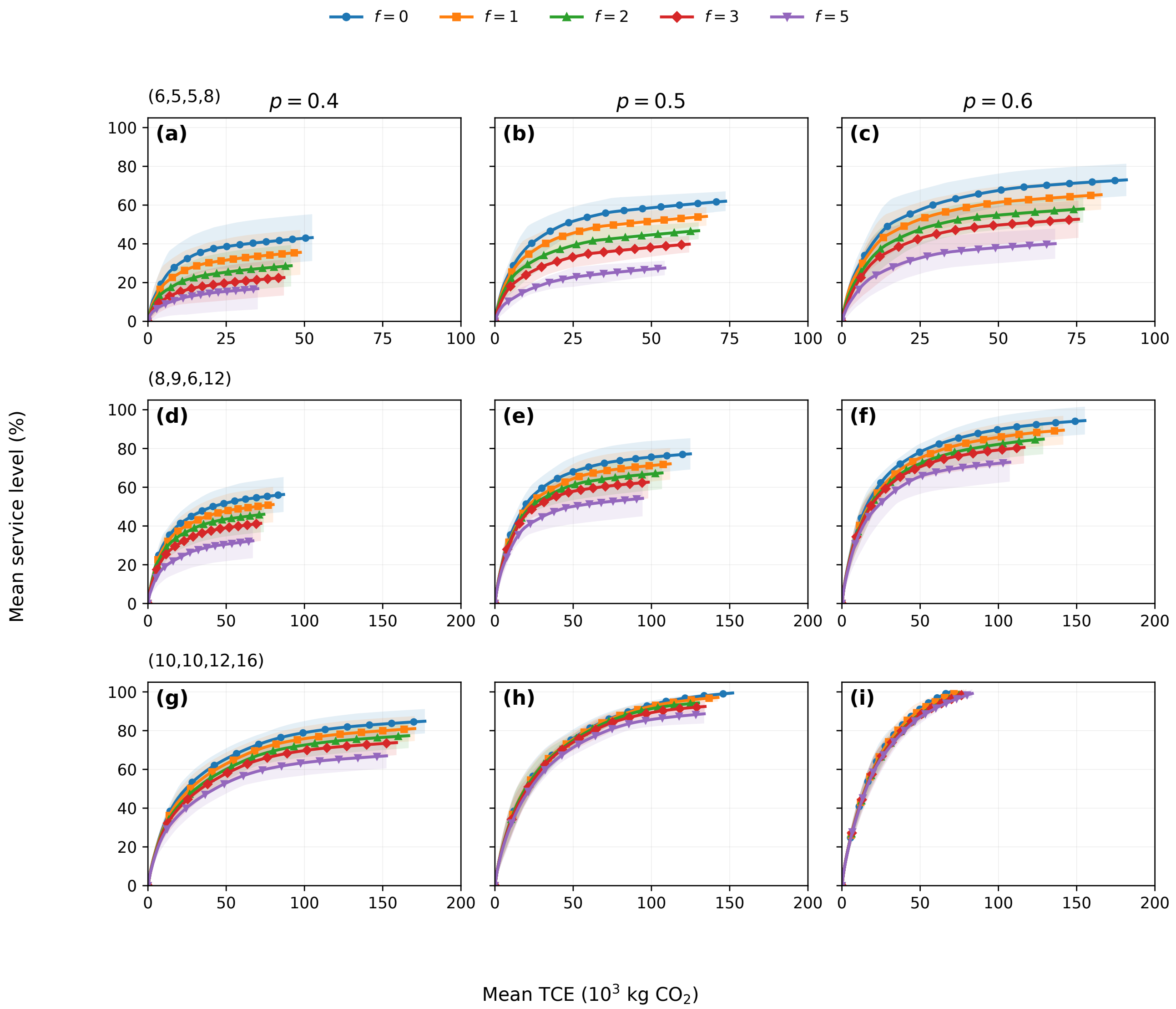

Figure 4. Mean service–carbon tradeoffs across SCN sizes and $p \in \{0.4, 0.5, 0.6\}$, with 95% confidence intervals. Rows correspond to $(|S|, |P|, |W|, |R|) = (6, 5, 5, 8)$, $(8, 9, 6, 12)$, and $(10, 10, 12, 16)$; columns correspond to $p \in \{0.4, 0.5, 0.6\}$.

5.4. Sensitivity to emission factors, demand, and mode composition (Experiment from Section 4.2)

Table 7 reports TLD at $\epsilon/\epsilon_{\text{Max}} = 0.50$ for $f \in \{0, 1, 2, 3, 5\}$; the complete experiments additionally evaluate $\epsilon/\epsilon_{\text{Max}} \in \{0, 0.25, 0.50, 0.75, 1.00\}$. Because ϵ_{Max} is computed separately for each parameter specification, these normalized levels represent corresponding relative positions along each case's emission limit range rather than common absolute TCE limits. Changing the emission factors alters the carbon scale and recovery along the frontier but not the carbon unconstrained service endpoint, because these factors affect emission accounting rather than physical capacity. At $\epsilon/\epsilon_{\text{Max}} = 0.50$ and $f = 5$, for example, TLD is 680.14, 666.77, and 665.26 under the lower contrast, baseline, and higher contrast specifications, respectively. Demand produces substantial quantitative shifts while preserving the disruption ordering. At $f = 5$ and $\epsilon/\epsilon_{\text{Max}} = 0.50$, TLD increases from 458.90 under $0.8D$ to

666.77 under D and 874.57 under $1.2D$. Thus, greater demand pressure shifts the frontier toward higher lost demand without changing the qualitative effect of increasing disruption. Mode composition also materially affects performance because mode determines both capacity and distance adjusted emission intensity. At $f = 5$ and $\epsilon/\epsilon_{\text{Max}} = 0.50$, TLD is 511.05, 666.77, and 775.30 for the rail-heavy, baseline, and road/air-heavy cases, respectively; the corresponding carbon unconstrained endpoints are 472.45, 606.00, and 733.04. These differences reflect the joint capacity and emission characteristics of the alternative mode compositions. Overall, the sensitivity experiments show that the principal service–carbon and disruption patterns persist across the tested parameter specifications, while the magnitude and distribution of recovery vary with emission factors, demand, and mode composition.

Table 7. Parameter sensitivity of TLD for the representative $p = 0.5$ network at $\epsilon/\epsilon_{\text{Max}} = 0.50$.

Dimension	Case	$f = 0$	$f = 1$	$f = 2$	$f = 3$	$f = 5$
Emission factor	Lower contrast	466.18	512.32	550.69	592.89	680.14
	Baseline	451.44	498.66	537.79	581.65	666.77
	Higher contrast	447.43	495.45	535.78	580.15	665.26
Demand	$0.8D$	244.94	292.23	331.99	375.48	458.90
	D	451.44	498.66	537.79	581.65	666.77
	$1.2D$	658.92	706.10	745.63	789.45	874.57
Mode composition	Rail-heavy	298.22	344.03	383.70	427.14	511.05
	Baseline	451.44	498.66	537.79	581.65	666.77
	Road/air-heavy	631.53	679.56	705.52	726.96	775.30

5.5. Robustness to disruption-scenario selection (Experiment from Section 4.3)

The principal analysis uses the max–min service worst disruption scenario as the adverse benchmark. Figures 5, 6, and 7 repeat the analysis using critical-link, random, and representative average random scenarios, respectively. The alternative scenario selection rules produce quantitatively different frontiers. This distinction is most evident under random disruption selection, where additional randomly located failures can have relatively limited impact when the affected links are not operationally consequential. Thus, the number of failed links alone does not determine the realized severity of a disruption; the location and operational significance of the failed links also influence the resulting service degradation. Despite these differences, the qualitative service–carbon behavior persists across the alternative scenario constructions: increasing permitted emissions reduces TLD toward the attainable service level, and the marginal improvement profiles continue to exhibit changes in marginal recovery along the tradeoff. Hence, the service–carbon tradeoff and changing marginal effectiveness of additional TCE are robust to the scenario selection rule, while the magnitude of service degradation depends on which links are disrupted. Therefore, the robustness analysis supports the qualitative tradeoff conclusions while also demonstrating that disruption location, rather than failure count alone, is important to determine the quantitative severity of service degradation.

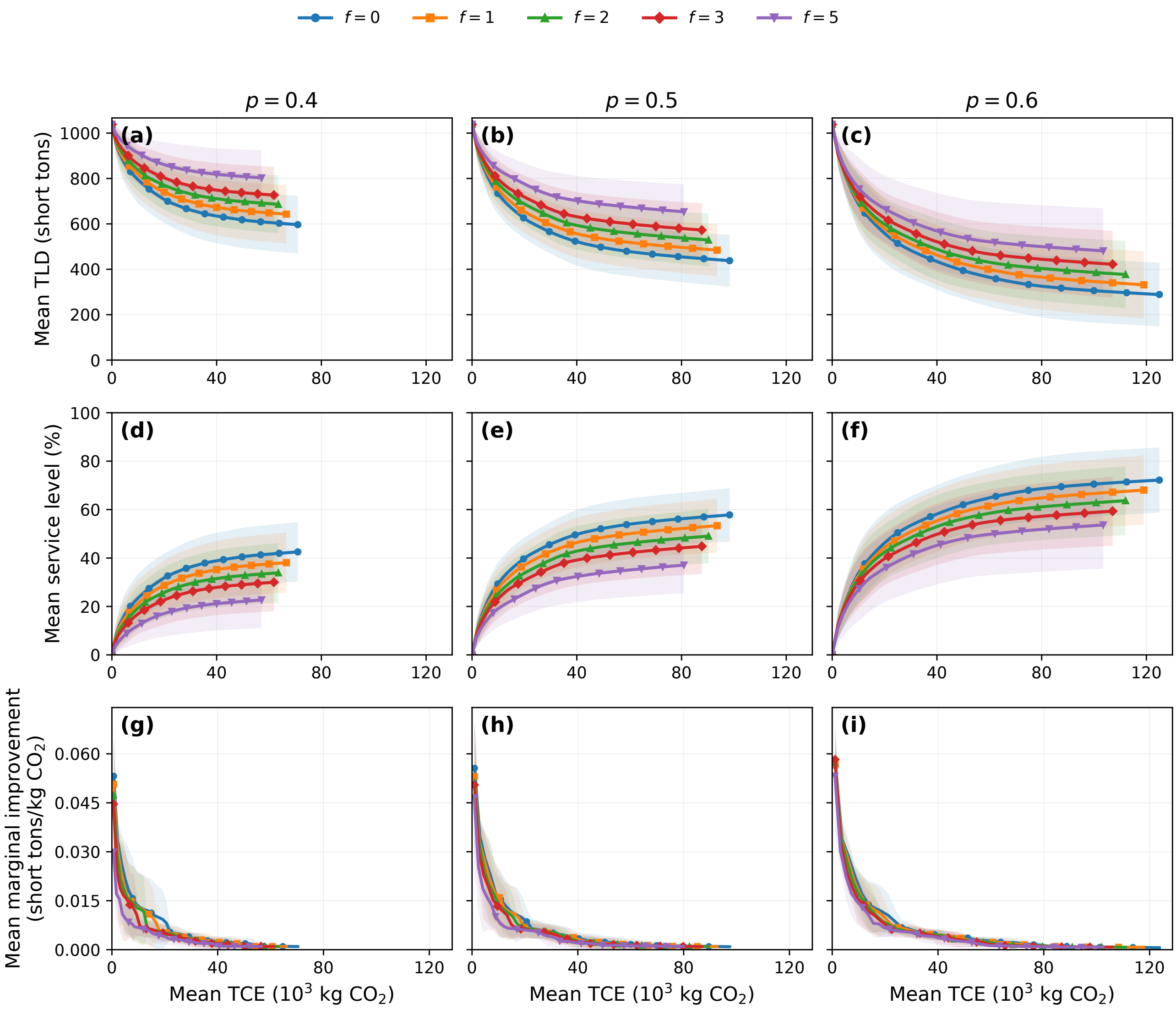

Figure 5. Service–carbon tradeoffs under *critical-link disruption* selection. Columns correspond to $p \in \{0.4, 0.5, 0.6\}$; rows report mean TLD, mean service level, and mean marginal improvement, respectively. Curves show means across ten independent network realizations for $f \in \{0, 1, 2, 3, 5\}$, with shaded regions representing 95% confidence intervals.

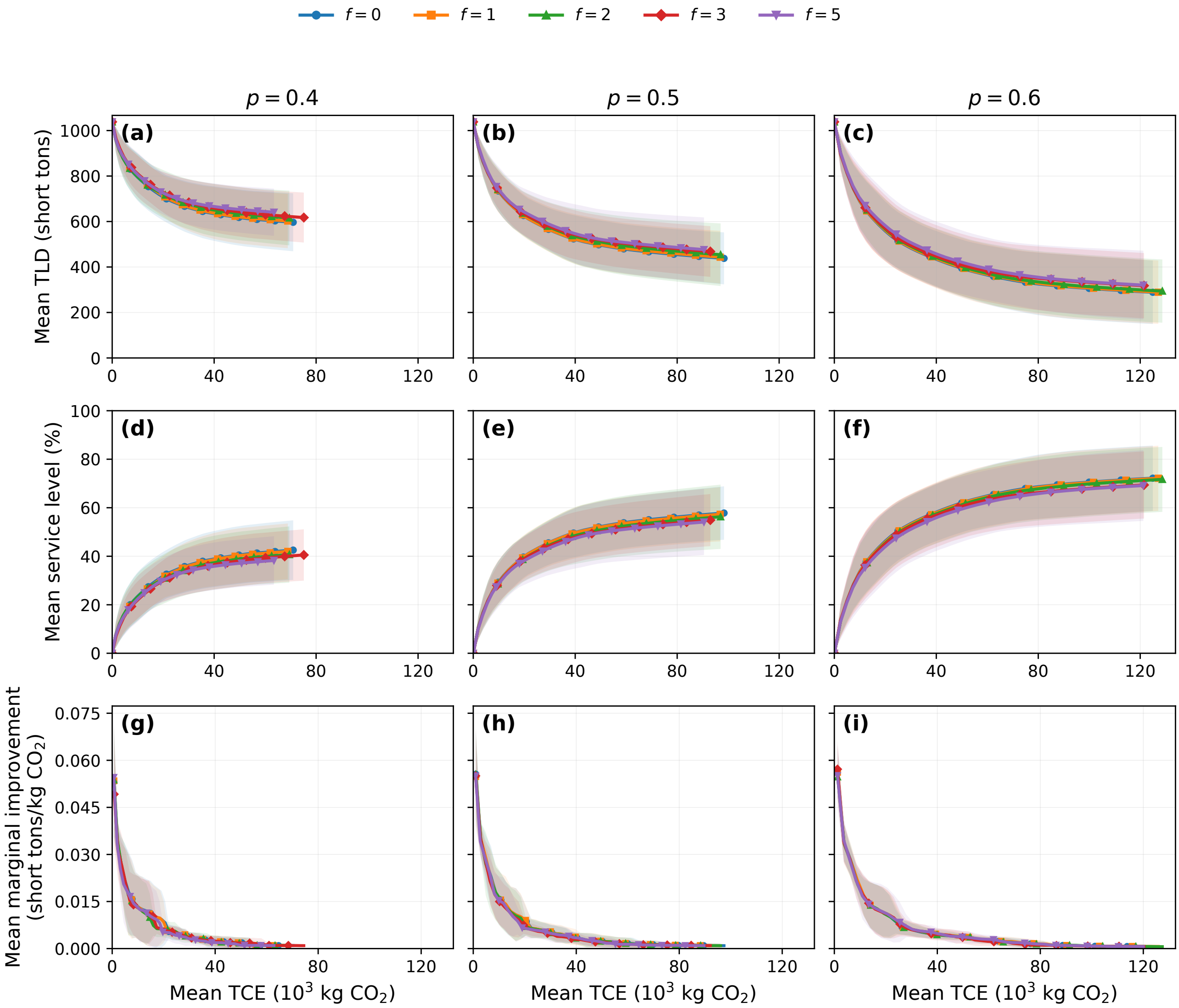

Figure 6. Service–carbon tradeoffs under *random disruption selection*. Columns correspond to $p \in \{0.4, 0.5, 0.6\}$; rows report mean TLD, mean service level, and mean marginal improvement, respectively. Curves show means across ten independent network realizations for $f \in \{0, 1, 2, 3, 5\}$, with shaded regions representing 95% confidence intervals.

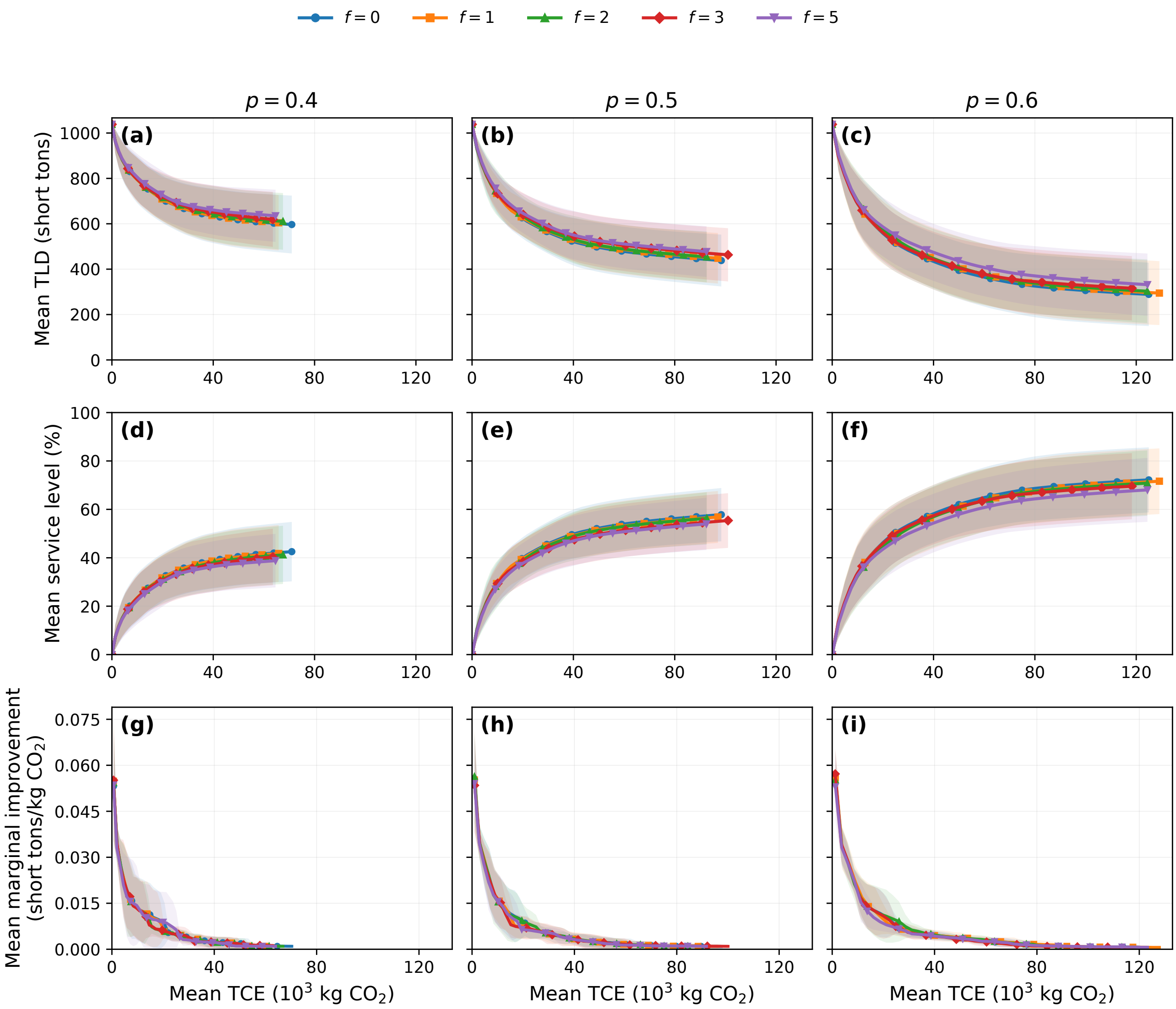

Figure 7. Service–carbon tradeoffs under *representative-average random disruption selection*. Columns correspond to $p \in \{0.4, 0.5, 0.6\}$; rows report mean TLD, mean service level, and mean marginal improvement, respectively. Curves show means across ten independent network realizations for $f \in \{0, 1, 2, 3, 5\}$, with shaded regions representing 95% confidence intervals.

5.6. Managerial interpretation

The results provide several implications for sustainability constrained disruption management in capacity-constrained operating environments. Because the experiments use synthetic SCNs calibrated to represent networks already operating under capacity pressure, the managerial implications below concern the comparative effects of the disruption severity, network structure, and emission restrictions rather than the specific numerical service levels as universal benchmarks for real-world SCNs. First, emission flexibility should be used as a targeted recovery lever rather than viewed as uniformly beneficial. Marginal improvement profiles illustrate portions of the tradeoff where relaxing the emission limit produces relatively larger service gains and where those gains diminish. Because declines toward lower marginal improvement generally occur earlier under larger max–min failure budgets in the tested instances, managers can use these profiles to assess when additional permitted emissions remain operationally valuable. Second, resilience investments should consider how connectivity is distributed, not simply how many links are available. Degree-balanced networks generally outperform hub-dominated networks even when node sets, link counts, and link-attribute multisets are controlled. Thus, distributing alternative routes across intermediate nodes can preserve the recovery capability without necessarily adding links or aggregate capacity, whereas excessive dependence on highly connected hubs can increase the vulnerability. Third, disruption preparedness should account for the structural context of the network. The effects of the selected failures generally diminish as routing alternatives increase in larger and denser networks. Hence, the same failure budget can have substantially different service consequences across networks, and investments in the routing redundancy can reduce the operational impact of link failures. Fourth, managers should distinguish environmental accounting changes from changes in the physical recovery capability. Changing the emission factors alters the carbon scale and the distribution of recovery along the frontier but, with the capacities fixed, does not change the carbon unconstrained service endpoint. Contrastingly, the demand and mode composition can also change the capacity pressure and attainable service. Therefore, the environmental policy parameters should not be interpreted as direct measures of the network's physical recovery capability. Finally, the disruption risk should not be assessed by failure count alone. The alternative scenario selection experiments show that the service impact of a given failure budget depends materially on which links fail. Therefore, resilience planning should combine failure count measures with link criticality assessments to identify and protect transportation connections with the greatest operational consequences. Overall, effective sustainability constrained recovery requires coordinating emission flexibility, routing redundancy, capacity planning, and protection of critical links.

6. Conclusion

This paper developed a prescriptive analytics framework to characterize the service–carbon tradeoff in disrupted multi-echelon SCNs. The computational analysis shows that disruption affects both the attainable service and the marginal effectiveness of recovery. Under the principal max–min analysis, larger failure budgets are generally associated with worse service outcomes and earlier declines toward lower marginal improvement levels. The expanded experiments further establish that these tradeoffs are sensitive to the network density, topology, size, and operating parameters, while remaining qualitatively robust across alternative fixed disruption scenario selection rules. Importantly, the results also show that the quantitative effect of disruption depends on the failed link configuration rather than on failure count alone. The study is limited to synthetic networks, link failure disruptions, and transportation related emissions, without explicitly modeling the cost, lead time, or other operational criteria. Future work can extend the framework to empirically calibrated networks, additional operational objectives and disruption mechanisms, and endogenous network design decisions. An additional direction is emission limit dependent adversarial analysis in which the disruption scenario is reoptimized along the service–carbon frontier.

Author contributions

Ashish Chandra: Conceptualization, Methodology, Formal analysis, Investigation, Software, Validation, Visualization, Writing – original draft, Writing – review and editing.

Data availability

No real-world data were used in this study. All computational results are based on synthetically generated instances described in the manuscript.

Conflicts of interest

The author declares that they have no conflict of interest.

Use of Generative-AI tools declaration

The authors declare that no generative artificial intelligence tools were used in the preparation, writing, editing, analysis, or creation of this article.

References

1. S. Benjaafar, Y. Li, M. Daskin, Carbon footprint and the management of supply chains: Insights from simple models, *IEEE Trans. Autom. Sci. Eng.*, **10** (2013), 99–116. https://doi.org/10.1109/TASE.2012.2203304
2. A. Chaabane, A. Ramudhin, M. Paquet, Design of sustainable supply chains under the emission trading scheme, *Int. J. Prod. Econ.*, **135** (2012), 37–49. https://doi.org/10.1016/j.ijpe.2010.10.025
3. X. Wang, G. Chen, S. Xu, Bi-objective green supply chain network design under disruption risk through an extended nsga-ii algorithm, *Clean. Logist. Supply Chain*, **3** (2022), 100025. https://doi.org/10.1016/j.clscn.2021.100025
4. N. Foroozesh, B. Karimi, S. Mousavi, Green-resilient supply chain network design for perishable products considering route risk and horizontal collaboration under robust interval-valued type-2 fuzzy uncertainty: A case study in food industry, *J. Environ. Manage.*, **307** (2022), 114470. https://doi.org/10.1016/j.jenvman.2022.114470
5. O. Badejo, M. Ierapetritou, A mathematical modeling approach for supply chain management under disruption and operational uncertainty, *AIChE J.*, **69** (2023), e18037. https://doi.org/10.1002/aic.18037
6. A. Kumar, K. Kumar, An uncertain sustainable supply chain network design for regulating greenhouse gas emission and supply chain cost, *Clean. Logist. Supply Chain*, **10** (2024), 100142. https://doi.org/10.1016/j.clscn.2024.100142
7. R. Yuniarti, Suparno, N. I. Arvitrida, A scoping review and bibliometric analysis of sustainable and resilient supply chain network design, *Supply Chain Anal.*, **12** (2025), 100162. https://doi.org/10.1016/j.sca.2025.100162

8. S. Ghorbani, J. Nematian, F. Yıldırım, S. A. Vurdu, A risk-averse multi-objective analytics framework for green supply chain design under uncertainty, *Supply Chain Anal.*, **13** (2026), 100199. https://doi.org/10.1016/j.sca.2026.100199

9. X. X. Zhu, M. H. Ran, D. Regan, A hybrid complex network-ml approach for critical state identification and mitigation in emergency supply chain cascading failures, *Reliab. Eng. Syst. Saf.*, **275** (2026), 112796. https://doi.org/10.1016/j.ress.2026.112796

10. Y. Bouchery, A. Ghaffari, Z. Jemai, Y. Dallery, Including sustainability criteria into inventory models, *Eur. J. Oper. Res.*, **222** (2012), 229–240. https://doi.org/10.1016/j.ejor.2012.05.004

11. L. Sánchez-Pravos, J. Parra-Domínguez, S. R. González, P. Chamoso, A machine learning and evolutionary optimization framework for carbon-aware supply chain routing, *Supply Chain Anal.*, **13** (2026), 100182. https://doi.org/10.1016/j.sca.2025.100182

12. A. Saurav, V. Yadav, C. Shekhar, An inventory optimization model for reliable and sustainable supply chains under trade credit and carbon constraints, *Supply Chain Anal.*, **11** (2025), 100132. https://doi.org/10.1016/j.sca.2025.100132

13. C. S. Tang, Robust strategies for mitigating supply chain disruptions, *Int. J. Logist. Res. Appl.*, **9** (2006), 33–45. https://doi.org/10.1080/13675560500405584

14. B. Adenso-DÃaz, J. Mar-Ortiz, S. Lozano, Assessing supply chain robustness to links failure, *Int. J. Prod. Res.*, **56** (2018), 5104–5117. https://doi.org/10.1080/00207543.2017.1419582

15. K. Zhao, K. Scheibe, J. Blackhurst, A. Kumar, Supply chain network robustness against disruptions: Topological analysis, measurement, and optimization, *IEEE Trans. Eng. Manage.*, **66** (2019), 127–139. https://doi.org/10.1109/tem.2018.2808331

16. A. Tolooie, M. Maity, A. K. Sinha, A two-stage stochastic mixed-integer program for reliable supply chain network design under uncertain disruptions and demand, *Comput. Ind. Eng.*, **148** (2020), 106722. https://doi.org/10.1016/j.cie.2020.106722

17. K. Katsaliaki, P. Galetsi, S. Kumar, Supply chain disruptions and resilience: a major review and future research agenda, *Ann. Oper. Res.*, **319** (2021), 965–1002. https://doi.org/10.1007/s10479-020-03912-1

18. P. Suryawanshi, P. Dutta, Optimization models for supply chains under risk, uncertainty, and resilience: A state-of-the-art review and future research directions, *Transp. Res. Part E Logist. Transp. Rev.*, **157** (2022), 102553. https://doi.org/10.1016/j.tre.2021.102553

19. Z. Yuliu, R. Shi, M. G. Ierapetritou, Mathematical programming approaches to supply chain optimization under uncertainty: a review, *Curr. Opin. Chem. Eng.*, **51** (2026), 101207. https://doi.org/10.1016/j.coche.2025.101207

20. X. Zhu, J. Zhu, D. Regan, Z. Wen, Exploring cascading failures in supply chain risk management: A systematic review, 2013–2024, *J. Saf. Sci. Resil.*, **7** (2026), 100234. https://doi.org/10.1016/j.jnlssr.2025.100234

21. J. C. Smith, Y. Song, A survey of network interdiction models and algorithms, *Eur. J. Oper. Res.*, **283** (2020), 797–811. https://doi.org/10.1016/j.ejor.2019.06.024

22. A. Chandra, M. Tawarmalani, Probability estimation via policy restrictions, convexification, and approximate sampling, *Math. Program.*, **196** (2022), 309–345. https://doi.org/10.1007/s10107-022-01823-6
23. A. Chandra, J. G. Kim, Reliability certification of supply chain networks under uncertain failures and demand, *Ann. Oper. Res.*, **361** (2025), 1151–1181. https://doi.org/10.1007/s10479-025-06790-7
24. H. Golpîra, A. Javanmardan, Robust optimization of sustainable closed-loop supply chain considering carbon emission schemes, *Sustain. Prod. Consum.*, **30** (2022), 640–656. https://doi.org/10.1016/j.spc.2021.12.028
25. C. Savithi, C. Kaewta, Multi-objective optimization of gateway location selection in long-range wide area networks: A tradeoff analysis between system costs and bitrate maximization, *J. Sens. Actuator Netw.*, **13** (2024), 3. https://doi.org/10.3390/jsan13010003
26. S. Giannelos, X. Zhang, T. Zhang, G. Strbac, Multi-objective optimization for pareto frontier sensitivity analysis in power systems, *Sustainability*, **16** (2024), 5854. https://doi.org/10.3390/su16145854
27. M. Eskandarpour, P. Dejax, J. Miemczyk, O. Péton, Sustainable supply chain network design: An optimization-oriented review, *Omega*, **54** (2015), 11–32. https://doi.org/10.1016/j.omega.2015.01.006
28. F. Si, J. Wang, Y. Han, Q. Zhao, Risk-averse multiobjective optimization for integrated electricity and heating system: An augment epsilon-constraint approach, *IEEE Syst. J.*, **16** (2022), 5142–5153. https://doi.org/10.1109/JSYST.2021.3135295
29. H. Jiang, S. Zhang, Z. Ren, *Solving Multiobjective Optimization Problem by Constraint Optimization*, 637–646, Springer Berlin Heidelberg, 2010.
30. Y. Yao, Tri-level thinking: models of three-way decision, *Int. J. Mach. Learn. Cybern.*, **11** (2019), 947–959. https://doi.org/10.1007/s13042-019-01040-2
31. S. Khalifehzadeh, M. Seifbarghy, B. Naderi, A four-echelon supply chain network design with shortage: Mathematical modeling and solution methods, *J. Manuf. Syst.*, **35** (2015), 164–175. https://doi.org/10.1016/j.jmsy.2014.12.002
32. H. Rafiei, F. Safaei, M. Rabbani, Integrated production-distribution planning problem in a competition-based four-echelon supply chain, *Comput. Ind. Eng.*, **119** (2018), 85–99. https://doi.org/10.1016/j.cie.2018.02.031
33. A. Gharaei, S. H. R. Pasandideh, A. Arshadi Khamseh, Inventory model in a four-echelon integrated supply chain: modeling and optimization, *J. Model. Manag.*, **12** (2017), 739–762. https://doi.org/10.1108/JM2-07-2016-0065
34. M. Sebatjane, O. Adetunji, A four-echelon supply chain inventory model for growing items with imperfect quality and errors in quality inspection, *Ann. Oper. Res.*, **335** (2023), 327–359. https://doi.org/10.1007/s10479-023-05501-4
35. E. H. Sabri, B. M. Beamon, A multi-objective approach to simultaneous strategic and operational planning in supply chain design, *Omega*, **28** (2000), 581–598. https://doi.org/10.1016/s0305-0483(99)00080-8

36. S. Zandkarimkhani, H. Mina, M. Biuki, K. Govindan, A chance constrained fuzzy goal programming approach for perishable pharmaceutical supply chain network design, *Ann. Oper. Res.*, **295** (2020), 425–452. https://doi.org/10.1007/s10479-020-03677-7

37. M. Taheri-Bavil-Oliaei, S. H. Zegordi, R. Tavakkoli-Moghaddam, Bi-objective build-to-order supply chain network design under uncertainty and time-dependent demand: An automobile case study, *Comput. Ind. Eng.*, **154** (2021), 107126. https://doi.org/10.1016/j.cie.2021.107126

38. U.S. Environmental Protection Agency, *2024 SmartWay Online Shipper Tool: Technical Documentation, U.S. Version 1.0 (Data Year 2023)*, Technical Report EPA-420-B-24-048, U.S. Environmental Protection Agency, Office of Transportation and Air Quality, 2024. Available from: https://www.epa.gov/nscep.

39. Gurobi Optimization, LLC, Gurobi Optimizer Reference Manual, 2023, Available from: https://www.gurobi.com.

AIMS Press